

# Nanocluster-Containing Mesoporous Magnetoceramics from Hyperbranched Organometallic Polymer Precursors<sup>†</sup>

Qunhui Sun,<sup>‡</sup> Jacky W. Y. Lam,<sup>‡</sup> Kaitian Xu,<sup>‡</sup> Hongyao Xu,<sup>‡</sup> John A. K. Cha,<sup>‡</sup> Philip C. L. Wong,<sup>§</sup> Gehui Wen,<sup>||</sup> Xixiang Zhang,<sup>||</sup> Xiabin Jing,<sup>⊥</sup> Fosong Wang,<sup>⊥</sup> and Ben Zhong Tang<sup>\*,‡</sup>

Department of Chemistry, Materials Characterization and Preparation Facility, and Department of Physics, Hong Kong University of Science & Technology, Clear Water Bay, Kowloon, Hong Kong, China, and Changchun Institute of Applied Chemistry, Chinese Academy of Sciences, Changchun, China

Received February 3, 2000. Revised Manuscript Received June 20, 2000

Pyrolysis of hyperbranched poly[1,1'-ferrocenylene(methyl)silylene] (**5**) yields mesoporous, conductive, and magnetic ceramics (**6**). Sintering at high temperatures (1000–1200 °C) under nitrogen and argon converts **5** to **6N** and **6A**, respectively, in ~48–62% yields. The ceramization yields of **5** are higher than that (~36%) of its linear counterpart poly[1,1'-ferrocenylene(dimethyl)silylene] (**1**), revealing that the hyperbranched polymer is superior to the linear one as a ceramic precursor. The ceramic products **6** are characterized by SEM, XPS, EDX, XRD, and SQUID. It is found that the ceramics are electrically conductive and possess a mesoporous architecture constructed of tortuously interconnected nanoclusters. The iron contents of **6** estimated by EDX are 36–43%, much higher than that (11%) of the ceramic **2** prepared from the linear precursor **1**. The nanocrystals in **6N** are mainly  $\alpha$ -Fe<sub>2</sub>O<sub>3</sub> whereas those in **6A** are mainly Fe<sub>3</sub>Si. When magnetized by an external field at room temperature, **6A** exhibits a high-saturation magnetization ( $M_s \sim 49$  emu/g) and near-zero remanence and coercivity; that is, **6A** is an excellent soft ferromagnetic material with an extremely low hysteresis loss.

## Introduction

The use of chemical approaches to create new nanostructured morphologies and to tune chemical and physical properties of ceramic materials is a rapidly growing area of research.<sup>1</sup> The vigorous research activity in the synthesis of organometallic polymer precursors and their controlled pyrolysis to ceramic materials has opened up a new branch of macromolecular science—preceramic polymer chemistry.<sup>2</sup> The polymer precursor

route offers the following, among other, noteworthy advantages: (i) the diversity in chemical compositions of organometallic macromolecules provides a large palette for manipulating the structure and properties of the ceramic products, (ii) the inorganic metal atoms distributed along the macromolecular chains and segregated by the organic moieties can, upon pyrolysis, form nanoclusters, interconnection of which may generate mesoporous morphologies; and (iii) the unique processing characteristics of the precursor polymers may enable the fabrication of bulk ceramic bodies of complex shapes. Not all these advantages have, however, been realized or utilized, and indeed, most studies in the preceramic polymer chemistry have been so far concentrated on the fabrication of structural ceramics with outstanding mechanical properties, examples of which include silicon carbide (SiC) and silicon nitride (Si<sub>3</sub>N<sub>4</sub>).<sup>3</sup> Incorporation of nanoclusters of transition metals into

<sup>†</sup> Parts of this work were reported at the 1999 Fall and 2000 Spring ACS Meetings (ref 6).

\* To whom correspondence should be addressed. E-mail: tangbenz@ust.hk.

<sup>‡</sup> Department of Chemistry, Hong Kong University of Science & Technology.

<sup>§</sup> Materials Characterization and Preparation Facility, Hong Kong University of Science & Technology.

<sup>||</sup> Department of Physics, Hong Kong University of Science & Technology.

<sup>⊥</sup> Chinese Academy of Sciences.

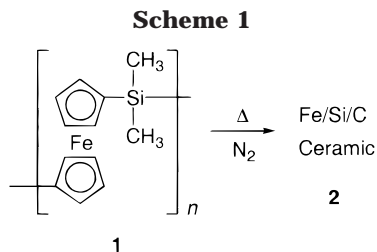
(1) For selected reviews and monographs, see: (a) Ozin, G. A. *Chem. Commun.* **2000**, 419. (b) *Nanostructured Materials*; Jena, P., Ed.; Nova Science: New York, 1996. (c) Mann, S.; Ozin, G. A. *Nature* **1996**, *382*, 313. (d) *Application of Organometallic Chemistry in the Preparation and Processing of Advanced Materials, NATO ASI Series E*; Harrod, J. F., Laine, R. M., Eds.; Kluwer Academic Press: Dordrecht, The Netherlands, 1995. (e) Whitesides, G. M. *Sci. Am.* **1995**, *273*, 146. (f) *Integrated Chemical Synthesis, A Chemical Approach to Nanotechnology*; Bard, A. J., Ed.; Wiley: New York, 1994. (g) Dagani, R. *Chem. Eng. News* **1992**, *70* (47), 18. (h) Segal, D. *Chemical Synthesis of Advanced Ceramic Materials*; Cambridge University Press: New York, 1991. (i) Schaefer, D. *Science* **1989**, *243*, 1023. (j) *Better Ceramics through Chemistry II*; Brinkler, C. J., D. E., Ulrich, D. R., Eds.; MRS: Pittsburgh, PA, 1986.

(2) (a) Chan, V. Z.-H.; Hoffman, J.; Lee, V. Y.; Latrou, H.; Avgeropoulos, A.; Hadjichristidis, N.; Miller, R. D.; Thomas, E. L. *Science* **1999**, *286*, 1716. (b) Rice, R. W. *CHEMTECH* **1983**, *13*, 230. For selected reviews and monographs, see: (c) Wynne, K. J.; Rice, R. W. *Annu. Rev. Mater. Sci.* **1994**, *14*, 297. (d) Seyferth, D. In *Silicon-Based Polymer Science*; Ziegler, J. M., Fearon, F. W. G., Eds.; American Chemical Society: Washington, DC, 1990; Chapter 31. (e) Paine, R. T.; Narula, C. K. *Chem. Rev.* **1990**, *90*, 73.

(3) (a) Messier, D. R.; Croft, W. J. In *Preparation and Properties of Solid State Materials*; Wilcox, W. R., Eds.; Dekker: New York, 1982; Vol. 7, Chapter 2. (b) *Gmelin Handbook of Inorganic Chemistry*, 8th ed.; Springer-Verlag: Berlin, 1986; Silicon, Suppl. Vol. B3. (c) Yajima, S.; Hayashi, Momori, M.; Okamura, K. *Nature* **1976**, *261*, 683.

ceramics may lead to the development of novel nanostructured materials with unique magnetic, electrical, and optical properties. Such possibility, intriguing notwithstanding, has not been well explored.

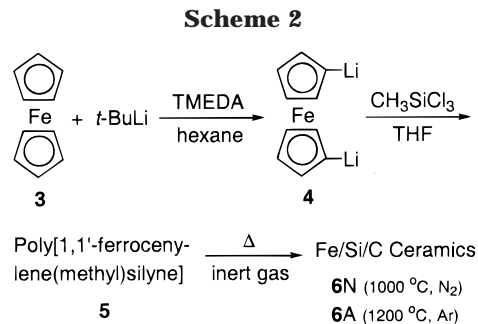
In 1993, Manners and co-workers prepared iron-, silicon-, and carbon-containing ceramic **2** by the controlled pyrolysis of poly([1]silaferrocenophane) **1** (Scheme 1).<sup>4</sup> The ceramic was magnetizable and exhibited a



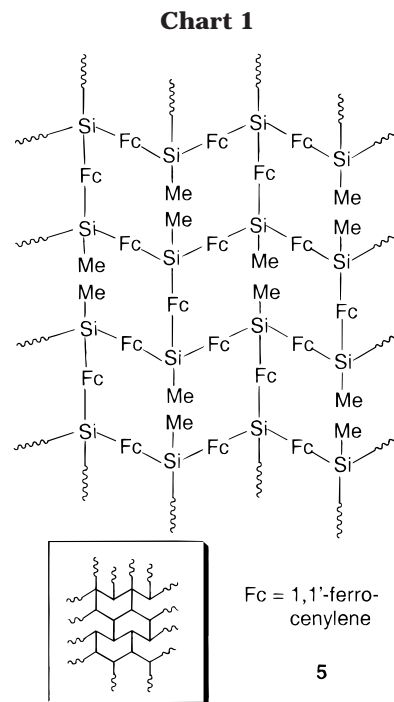
saturation magnetization ( $M_s$ ) of  $\sim 3.5$  emu/g.<sup>4c</sup> Pyrolysis of **1** inside the channels of mesoporous silica templates led to the formation of iron nanoparticles, whose  $M_s$  values were in the range of 0.52–1.84 emu/g.<sup>5a,b</sup> A recent exciting development in the area is the high-yield synthesis of shaped ceramics from cross-linked network polymers of spirocyclic [1]silaferrocenophane, whose magnetic properties could be readily tuned between superparamagnetic and ferromagnetic states by controlling the pyrolysis conditions.<sup>5c</sup>

Hyperbranched polymers are different from linear ones in terms of the dimensionality of molecular architecture, the former being three-dimensional spheres while the latter is one-dimensional chains. Compared to the open chains, the closed spheres should in principle better retain the constituent elements during the pyrolysis process, thus giving higher ceramic yields. Hyperbranched polymers are also different from cross-linked networks, the former often being soluble whereas the latter is inherently insoluble. Processibility is one of the important advantages of the preceramic polymer processes and we thus tried to explore the possibility of using hyperbranched polymers as precursors for the preparation of advanced ceramic materials.

We have recently synthesized a series of new hyperbranched iron- and silicon-containing organometallic polymers, poly[1,1'-ferrocenylene(*n*-alkyl)silynes], by the polymerizations of 1,1'-dilithioferrocene ( $\text{FcLi}_2$ ) with *n*-alkyltrichlorosilanes [ $(\text{C}_n\text{H}_{2n+1})\text{Cl}_3\text{Si}$ ;  $n = 1, 8, 12, 16, 18$ ].<sup>6</sup> The reaction scheme for one of the polysilynes, poly[1,1'-ferrocenylene(methyl)silyne] (**5**), is given in Scheme 2, and the diagrammatic illustration of its molecular structure is shown in Chart 1. In the hyper-



branched polymer **5**, every one of the silicon atoms is surrounded on the average by 3/2 (or 1.5) ferrocenylene moieties, and its theoretical iron content is thus higher



than that of its linear counterpart **1**, in whose monomer (repeat) unit one silicon is linked with only one (1) ferrocenylene group. The pyrolysis of **1** gave volatile fragmentation byproducts such as cyclic silaferrocenophanes, which sublimed out from the sintering system, contributing to the low iron content of **2**.<sup>4</sup> The three-dimensional molecular structure of **5** may suppress the iron loss caused by the volatilization, enhance the chances for the iron atoms to participate in the network formation, and hence increase the iron content of the ceramic end products.

With these considerations in mind, in this work, we investigated ceramization of the hyperbranched polysilynes. The pyrolysis of **5** produces ceramics **6** (Scheme 2), which possess mesoporous morphologies, contain large amounts of iron nanoclusters, and exhibit soft ferromagnetism with negligibly small hysteresis loss.

## Experimental Section

**Materials and Instrumentation.** Ferrocene was purchased from Aldrich and was further purified by recrystallization and sublimation in our laboratories. The *n*-alkyltrichlorosilanes, i.e., methyltrichlorosilane (Aldrich), *n*-hexyltrichlorosilane (United Chemical Technology), *n*-octyltrichlorosilane (Lancaster), *n*-dodecyltrichlorosilane (United Chemical Technol-

(4) (a) Tang, B. Z.; Petersen, R.; Foucher, D. A.; Lough, A.; Coombs, N.; Sodhi, R.; Manners, I. *J. Chem. Soc., Chem. Commun.* **1993**, 523.

(b) Foucher, D. A.; Ziembinski, R.; Tang, B. Z.; McDonald, P. M.; Massey, J.; Jaeger, C. R.; Vancso, G. J.; Manners, I. *Macromolecules* **1993**, *26*, 2878. (c) Petersen, R.; Foucher, D. A.; Tang, B. Z.; Lough, A.; Raju, N.; Greedan, J.; Manners, I. *Chem. Mater.* **1995**, *7*, 2045.

(5) (a) McLachlan, M. J.; Aroca, P.; Coombs, N.; Manners, I.; Ozin, G. A. *Adv. Mater.* **1998**, *10*, 144. (b) McLachlan, M. J.; Ginzburg, M.; Coombs, N.; Raju, N. P.; Greedan, J. E.; Ozin, G. A.; Manners, I. *J. Am. Chem. Soc.* **2000**, *122*, 3878. (c) MacLachlan, M. J.; Ginzburg, M.; Coombs, N.; Coyle, T. W.; Raju, N. P.; Greedan, J. E.; Ozin, G. A.; Manners, I. *Science* **2000**, *287*, 1460.

(6) (a) Sun, Q.; Tang, B. Z. *Polym. Prepr.* **1999**, *40*(2), 657. (b) Sun, Q.; Tang, B. Z. *Polym. Mater. Sci. Eng.* **2000**, *82*, 105. (c) Sun, Q.; Wen, G. H.; Zhang, X. X.; Tang, B. Z. *Polym. Mater. Sci. Eng.* **2000**, *82*, 107. (d) Sun, Q.; Tang, B. Z. *Polym. Mater. Sci. Eng.* **2000**, *82*, 109.

ogy), *n*-hexadecyltrichlorosilane (United Chemical Technology), and *n*-octadecyltrichlorosilane (Lancaster), were distilled over calcium hydride before use. *N,N,N,N*-Tetramethylethylenediamine (TMEDA; Acros), diethyl ether, hexane, and tetrahydrofuran (THF) (all from Lab-Scan) were distilled from sodium benzophenone ketyl or calcium hydride. *tert*-Butyllithium (1.7 M in heptane) and all other reagents and solvents were purchased from Aldrich and used as received without further purification.

Infrared spectra were measured on a Perkin-Elmer 16 PC FT-IR spectrophotometer.  $^1\text{H}$  and  $^{13}\text{C}$  NMR spectra were recorded on a Bruker ARX 300 spectrometer using chloroform-*d* as the solvent and tetramethylsilane (TMS;  $\delta = 0$ ) or chloroform (7.26) as the internal reference. Electronic absorption spectra were measured on a Milton Roy Spectronic 3000 diode array UV-vis spectrophotometer and the molar absorptivities ( $\epsilon$ ) of the polymers were calculated on the basis of their repeat (monomer) units. Molecular weights ( $M_w$  and  $M_n$ ) and polydispersity indexes ( $M_w/M_n$ ) of the polymers were estimated by a Waters Associates gel permeation chromatograph (GPC) system. THF was used as an eluent at a flow rate of 1.0 mL/min. A set of Waters monodisperse polystyrene standards covering the molecular weight range of  $10^3$ – $10^7$  were used for the molecular weight calibration. Differential scanning calorimetry (DSC) and thermogravimetric analysis (TGA) were performed on a Setaram DSC 92 and a Perkin-Elmer TGA 7, respectively, at a heating rate of  $10^\circ\text{C}/\text{min}$  under nitrogen.

Morphologies of the ceramic products were investigated on a JEOL 6300 scanning electron microscope (SEM) operating at an accelerating voltage of 5 kV, and the as-prepared ceramics were directly used in the SEM analysis without coating with gold metal. Energy-dispersion X-ray (EDX) analyses were performed on a Philips XL30 SEM system with quantitative elemental mapping and line scan capacities operating at an accelerating voltage of 15 kV. X-ray photoelectron spectroscopy (XPS) measurements were conducted on a PHI 5600 spectrometer (Physical Electronics) and the core level spectra were measured using a monochromatic Al  $K\alpha$  X-ray source ( $h\nu = 1486.6$  eV). The analyzer was operated at 23.5 eV pass energy and the analyzed area was  $800\ \mu\text{m}$  in diameter. Binding energies were referenced to the adventitious hydrocarbon C 1s line at 285.0 eV and curve fitting of the XPS spectra was performed using the least-squares method.<sup>7</sup> X-ray diffraction (XRD) diagrams were recorded on a Philips PW 1830 powder diffractometer using a monochromatized X-ray beam from nickel-filtered Cu  $K\alpha$  radiation ( $\lambda = 1.5406$  Å). Magnetization measurements were carried out using a superconducting quantum interference device (SQUID) magnetometer (Quantum Design MPMS-5S) at fields ranging from 0 to 20 kOe and at temperatures of 5 and 300 K.

**Synthesis of Polysilynes.** The detailed synthetic procedures and characterization data for the hyperbranched poly-[1,1'-ferrocenylene(*n*-alkyl)silylene] are reported elsewhere.<sup>6</sup> Typical examples for the preparation of two polysilyne samples are given below:

*Poly[1,1'-ferrocenylene(methyl)silylene] (5)*. Into a dry 100-mL three-necked round-bottom flask at room temperature under nitrogen with stirring were added 1.25 g (6.7 mmol) of ferrocene, 1.0 mL of TMEDA, 15 mL of hexane, and 8.0 mL (13.6 mmol) of *t*-BuLi (1.7 M in pentane). The mixture was stirred for 8 h at room temperature and then cooled to  $-78^\circ\text{C}$  with a dry ice/acetone bath. Methyltrichlorosilane (0.53 mL, 4.5 mmol) in 50 mL of THF was added and the reaction temperature was raised from  $-78^\circ\text{C}$  to room temperature in 4 h. The mixture was stirred for another 20 h at room temperature and the polymerization was then terminated by adding 0.2 mL of methanol. The mixture was filtered to remove the lithium chloride salt. The transparent solution was slightly concentrated and then added through a cotton filter into a large amount of methanol ( $\sim 1000$  mL) under stirring. The precipitate was isolated by filtration through a Gooch crucible, washed with methanol, and dried at room temperature under

vacuum to a constant weight. The polymeric product was obtained as golden yellow powdery solids in 71.1% yield.  $M_w = 2000$ ,  $M_w/M_n = 2.0$  (soluble fraction; GPC, polystyrene calibration). IR (KBr),  $\nu$  ( $\text{cm}^{-1}$ ): 3046, 1638, 1540, 1254, 1166, 1038, 788, 686.  $^1\text{H}$  NMR (300 MHz,  $\text{CDCl}_3$ ),  $\delta$  (TMS, ppm): 4.2 [( $\text{C}_5\text{H}_4$ ) $_2\text{Fe}$ ], 0.6 ( $\text{CH}_3$ ).  $T_g$  (DSC):  $53.1^\circ\text{C}$ . Temperature for 5% weight loss ( $T_{5\%}$ ; TGA):  $\sim 300^\circ\text{C}$ .

*Poly[1,1'-ferrocenylene(*n*-dodecyl)silylene]*. Into a dry flask were added 0.622 g (3.35 mmol) of ferrocene, 0.6 mL of TMEDA, 15 mL of hexane, and 4.0 mL (6.8 mmol) of *t*-BuLi (1.7 M in pentane) under nitrogen with stirring. The solution was stirred for 8 h at room temperature and was then cooled to  $-78^\circ\text{C}$ . Into the solution was added 0.67 mL (2.24 mmol) of *n*-dodecyltrichlorosilane in 50 mL of THF. The temperature was gradually raised to room temperature, the mixture was stirred for 24 h, and the polymerization was terminated by adding 0.2 mL of methanol. The polymerization product was isolated and purified by the same procedures detailed above for **5**. The polymer was obtained as amber powdery solids in 77.0% yield.  $M_w = 6300$ ,  $M_w/M_n = 3.8$  (GPC, polystyrene calibration). IR (KBr),  $\nu$  ( $\text{cm}^{-1}$ ): 2922, 2952, 1636, 1466, 1170, 1036, 688, 462.  $^1\text{H}$  NMR (300 MHz,  $\text{CDCl}_3$ ),  $\delta$  (TMS, ppm): 4.2 [( $\text{C}_5\text{H}_4$ ) $_2\text{Fe}$ ], 1.3 ( $\text{C}_{12}\text{H}_{25}$ ).  $^{13}\text{C}$  NMR (75 MHz,  $\text{CDCl}_3$ ),  $\delta$  (TMS, ppm): 73.1, 70.8, 67.9, 32.3, 31.9, 22.7, 14.1. UV ( $\text{CH}_2\text{-Cl}_2$ ),  $\lambda_{\text{max}}$ : 229 nm.  $\epsilon_{\text{max}}$ :  $6980\ \text{mol}^{-1}\ \text{L}\ \text{cm}^{-1}$ .  $T_g$  (DSC):  $-54.5^\circ\text{C}$ .  $T_{5\%}$  (TGA):  $\sim 306^\circ\text{C}$ .

**Preparation of Ceramics.** In one typical pyrolysis experiment conducted under nitrogen, 28 mg of **5** was placed in a sample cell of a Perkin-Elmer TGA 7 analyzer. The sample was heated to  $1000^\circ\text{C}$  at a heating rate of  $10^\circ\text{C}/\text{min}$  and calcinated at the highest temperature for 1 h. A ball-shaped ceramic product was obtained in  $\sim 50\%$  yield (referred to as **6N** with "N" standing for "nitrogen"). EDX, atomic composition (%): Fe, 36.0; Si, 24.4; C, 30.2; O, 9.4. XPS, atomic composition (%): Fe, 6.1; Si, 0.7; C, 78.0; O, 15.2. Binding energy (eV): Fe  $2p_{3/2}$ : 707.4, 712.3; Fe  $2p_{1/2}$ : 720.2, 725.8; Si  $2p$ : 104.0. (For assignments of the species with the core-level binding energies, see Tables 2 and 3.) XRD,  $2\theta$  (deg)/ $d$  spacing (Å): 19.00/4.67(9), 26.90/3.31(3), 28.45/3.13(4), 32.35/2.76(5), 33.00/2.71(2), 35.65/2.51(8), 38.45/2.34(0), 43.65/2.07(2), 44.55/2.03(3), 49.50/1.83(6), 51.00/1.79(2), 51.60/1.77(0), 54.75/1.67(6), 57.50/1.60(0), 59.85/1.54(2), 66.30/1.41(2), 67.40/1.38(7). (For assignments of the peaks associated with Bragg reflections of the nanocrystals  $\text{Fe}_3\text{Si}$ ,  $\text{Fe}_3\text{O}_4$ ,  $\alpha\text{-Fe}_2\text{O}_3$ ,  $\text{SiO}_2$ ,  $\text{SiC}$ , and C, see Table 4.) SQUID,  $M_s$  (emu/g): 21.3 (at 5 K), 15.9 (at 300 K). Remanence ( $M_r$ ; emu/g): 6.4 (5 K), 2.6 (300 K). Coercivity ( $H_c$ ; Oe): 180 (5 K), 65 (300 K).

In another typical pyrolysis experiment carried out under argon,  $\sim 40$  mg of **5** was placed in a quartz tube in a Winston-Salem Thermcraft furnace, which was heated to  $1200^\circ\text{C}$  at a heating rate of  $10^\circ\text{C}/\text{min}$  in a stream of argon (flow rate:  $\sim 200\ \text{cm}^3/\text{min}$ ). The sample was sintered at the temperature for 1 h, which gave a ceramic product in  $\sim 50\%$  yield (**6A**; "A" standing for "argon"). EDX, atomic composition (%): Fe, 43.2; Si, 29.1; C, 22.4; O, 5.3. XPS, atomic composition (%): Fe, 3.8; Si, 0.6; C, 86.7; O, 8.9. Binding energy (eV): Fe  $2p_{3/2}$ : 707.4, 710.8; Fe  $2p_{1/2}$ : 720.2, 724.8; Si  $2p$ : 99.9, 101.5, 104.0. (For assignments of the species with the core-level binding energies, see Tables 2 and 3.) XRD,  $2\theta$  (deg)/ $d$  spacing (Å): 26.50/3.36(4), 27.40/3.23(6), 30.40/2.93(7), 33.00/2.70(6), 35.48/2.52(8), 38.05/2.35(7), 40.75/2.21(1), 41.20/2.18(8), 45.40/1.99(6), 46.50/1.95(2), 59.95/1.54(2), 66.35/1.40(8), 69.00/1.36(0), 84.15/1.14(9). (For assignments of the peaks associated with Bragg reflections of the nanocrystals Fe,  $\text{Fe}_3\text{Si}$ ,  $\alpha\text{-Fe}_2\text{O}_3$ ,  $\gamma\text{-Fe}_2\text{O}_3$ ,  $\text{SiO}_2$ ,  $\text{SiC}$ , and C, see Table 4.) SQUID,  $M_s$  (emu/g): 51.3 (at 5 K), 48.6 (at 300 K), the  $M_r$  and  $H_c$  values at 5 and 300 K being all virtually nil ( $\sim 0$ ).

## Results and Discussion

**Pyrolysis.** The samples of the polysilyne **5** used in this study were prepared according to the polymerization reaction shown in Scheme 2.<sup>6</sup> The structure of the polymer was analyzed spectroscopically, and its  $^1\text{H}$  NMR spectrum is given in Figure 1 as an example of

(7) McIntyre, N. S.; Zetaruk, D. G. *Anal. Chem.* **1977**, *49*, 1521.

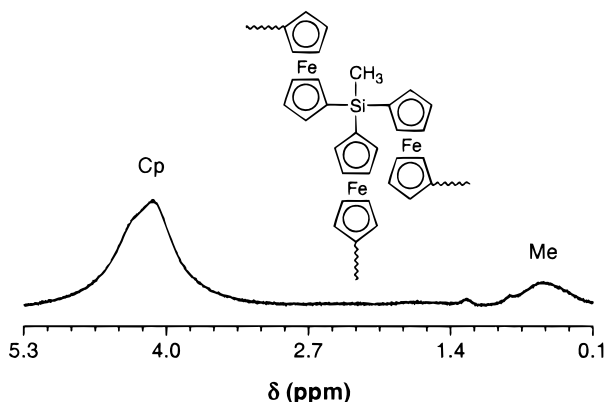


**Figure 1.**  $^1\text{H}$  NMR spectrum of chloroform- $d$  solution of hyperbranched poly[1,1'-ferrocenylene(methyl)silylene] **5**.

the characterization data. The protons of the cyclopentadienyl (Cp) rings exhibit a broad resonance peak centered at  $\delta$  4.2 and those of the methyl (Me) group resonate at  $\delta$  0.6. The repeat unit of **5** consists of 1.5 ferrocenylene  $\{[(\text{C}_5\text{H}_4)_2\text{Fe}]_{3/2}$  or  $\text{Fc}_{3/2}\}$  and 1 methyl ( $\text{CH}_3$ ) groups or 12 Cp and 3 Me protons. The ratio of the integrated areas of the observed Cp and Me peaks is 1:0.26, identical (within experimental error) to the theoretical value of 12:3 (or 1:0.25). For comparison, we prepared a linear polysilylene of similar structure **1** according to published procedures.<sup>8</sup> The NMR spectrum of **1** resembles that of **5** but the Cp/Me ratio of **1** is found to be 1:0.76 (theoretical value, 4:3 or 1:0.75). It thus becomes clear that the polysilylene **5** possesses the expected hyperbranched molecular structure. Using the same polymerization reaction, we prepared hyperbranched polysilylenes  $-\text{[Fc}_{3/2}\text{Si}(\text{C}_n\text{H}_{2n+1})]_p-$  with different lengths of alkyl chains ( $n$ ).<sup>6</sup> While **5** ( $n = 1$ ) is partially soluble, the polysilylenes with long alkyl chains ( $n \geq 8$ ) are completely soluble in common organic solvents such as THF and chloroform.

We first used TGA to investigate the pyrolysis of the hyperbranched polysilylenes under nitrogen. When  $n = 1$  (**5**), the pyrolysis gives a golden-colored ball-shaped ceramic product in the TGA cell in  $\sim 50\%$  yield. The ceramic yields of **5** vary in the range of  $\sim 48\text{--}62\%$  from batch to batch but are all higher than that ( $\sim 36\%$ ) of its linear counterpart **1**.<sup>4</sup> The pyrolysis yield monotonically decreases with an increase in the length of the alkyl chain. When  $n$  is increased to 12, the ceramic yields decrease to  $\sim 35\text{--}43\%$ , which are, however, still more than 2 times higher than that ( $\sim 17\%$ ) of its linear cousin with a similar number of carbon atoms, e.g., poly[1,1'-ferrocenylene(diphenyl)silylene].<sup>4</sup> Clearly, the hyperbranched polymers are superior to the linear ones in terms of thermolytic conversion to ceramic products. Cutting the backbone of a linear polymer a few times will quickly decrease its molecular weight, and volatilization of the low molecular weight fragments leads to a low ceramic yield.<sup>9,10</sup> On the other hand, breaking a few bonds of a hyperbranched polymer may not easily

change its polymeric nature because of its three-dimensional molecular architecture. The hyperbranched structure may even be viewed as a partial network, which should facilitate the cross-linking-induced ceramization, leading to an effective retention of the chain elements in the ceramic products. When a polymer possesses a complete network structure, it should give ceramic products in even higher yields, which is indeed the case, as elegantly demonstrated recently by Ozin and Manners' groups in their fabrication of magnetic ceramic materials from a cross-linked polysilylene in high yields ( $90 \pm 2\%$ ).<sup>5c</sup> Cross-linked network polymers are, however, completely insoluble; as ceramic precursors, they suffer from the disadvantage of poor processibility.

Since the polymer with the shortest alkyl chain length ( $n = 1$ ; **5**) gives the highest ceramic yields among all the hyperbranched poly[1,1'-ferrocenylene( $n$ -alkyl)silylenes],<sup>6</sup> we concentrated our research efforts on the development of ceramic materials from **5** and further studied its ceramization behaviors. When the samples of **5** are pyrolyzed in a furnace at  $1200^\circ\text{C}$  in a stream of argon, high ceramic yields ( $\sim 50\text{--}60\%$ ) are again obtained, confirming that the efficient ceramization is an intrinsic property of the hyperbranched polymer. IR analysis finds that the absorption bands of the organic groups in **5** are eliminated by the pyrolysis process. Clearly, the thermolysis has stripped the organic moieties, especially the hydrogen atoms, from the hyperbranched macromolecules, leaving the inorganic residue forming the thermosetting network of the ceramic products.<sup>9b</sup>

The SEM measurements of the ceramic products can be carried out without coating with gold metal. The clear images of the SEM photomicrographs indicate that the ceramics are electrically highly conductive, suggesting the existence of conductive graphite carbon and metallic iron species in the ceramic products. As can be seen from Figure 2, the ceramic looks like a coral reef in which the continuous skeletons are running through a mass of "islands" or clusters, many of which have sizes of a few hundred nanometers. On the two-dimensional imaging plane, the nanoclusters are separated by mesoscopic pores, but three dimensionally they are all tortuously interconnected, with the continuous skeletons providing the architectural support. Evidently, the coral-reef-like mesoporous structure is generated by the fast simultaneous evaporation of volatile organics and agglomeration of the inorganic elements in the pyrolysis process.

**Composition.** We used XPS spectroscopy to estimate the surface composition of the ceramic products. The XPS analysis finds four elements on the ceramic surface, namely, iron, silicon, carbon, and oxygen (Table 1). The Fe, Si, and C elements are understandably from the

(8) (a) Foucher, D. A.; Tang, B. Z.; Manners, I. *J. Am. Chem. Soc.* **1992**, *114*, 6246. (b) Finckh, W.; Tang, B. Z.; Foucher, D. A.; Zamble, D.; Ziembinski, R.; Lough, A.; Manners, I. *Organometallics* **1993**, *12*, 823. (c) Foucher, D. A.; Honeyman, C. H.; Nelson, J. M.; Tang, B. Z.; Manners, I. *Angew. Chem., Int. Ed. Engl.* **1993**, *32*, 1709. (d) Foucher, D. A.; Ziembinski, R.; Tang, B. Z.; McDonald, P.; Massey, J.; Raimund, J.; Vancso, J.; Manners, I. *Macromolecules* **1993**, *26*, 2878.

(9) (a) Interrante, L. V.; Whitmarsh, C. W.; Sherwood, W.; Wu, H.-J.; Lewis, R.; Maciel, G. In *Application of Organometallic Chemistry in the Preparation and Processing of Advanced Materials*, NATO ASI Series E; Harrod, J. F., Laine, R. M., Eds.; Kluwer Academic Press: Dordrecht, The Netherlands, 1995; Vol. 297, pp 173–183. (b) Liu, Q.; Wu, H.-J.; Lewis, R.; Maciel, G. E.; Interrante, L. V. *Chem. Mater.* **1999**, *11*, 2038.

(10) (a) Corriu, R. J. P.; Enders, M.; Huille, S.; Lusten, L.; Moreau, J. J. E. In *Application of Organometallic Chemistry in the Preparation and Processing of Advanced Materials*, NATO ASI Series E; Harrod, J. F., Laine, R. M., Eds.; Kluwer Academic Press: Dordrecht, The Netherlands, 1995; pp 185–199. (b) Atwell, W. H. In *Silicon-Based Polymer Science*; Ziegler, J. M., Fearon, F. W. G., Eds.; American Chemical Society: Washington, DC, 1990; Chapter 32.

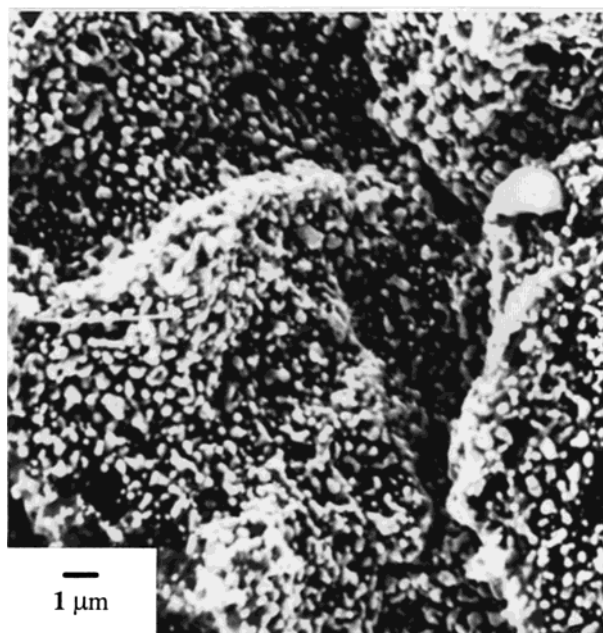


**Figure 2.** SEM photomicrograph of ceramic **6A** prepared by pyrolysis of **5** at 1200 °C under argon; scale bar: 1 μm (1000 nm).

**Table 1. Atomic Composition of Ceramics 6 Estimated by XPS and EDX Analyses**

ceramic	atomic composition (%)			
	Fe	Si	C	O
<b>6N</b> (XPS)	6.1	0.7	78.0	15.2
<b>6N</b> (EDX)	36.0	24.4	30.2	9.4
<b>6A</b> (XPS)	3.8	0.6	86.7	8.9
<b>6A</b> (EDX)	43.2	29.1	22.4	5.3

polymer precursor. Oxygen has often been found in the ceramic products prepared by the polymer precursor routes.<sup>2,3,11</sup> About 19% oxygen, for example, was detected in **2** by XPS, although the pyrolysis of **1** was conducted in a sealed quartz tube under nitrogen (cf. Scheme 1).<sup>4</sup> The iron nanoparticles of the ceramics generated inside the periodic mesoporous silica were also covered by oxide layers.<sup>5b</sup> The oxygenic species may be introduced by the moisture absorbed by the polymer samples prior to pyrolysis and/or by postoxidation of the mesoporous ceramics during the handling and storage processes.

The amounts of the Fe and Si elements in the bulk of the ceramics detected by the EDX analysis are much higher than those on the surface. On the other hand, there are smaller quantities of elemental C and O in the bulk than on the surface. This suggests that the ceramization process starts from the pyrolysis-induced formation of the inorganic metallic species. The nanoclusters shown in Figure 2 thus may be imagined as iron–silicon inner cores coated with carbonic and oxide outer layers.

An important piece of information offered by the elemental analyses is that both the ceramics prepared under nitrogen (**6N**) and argon (**6A**) comprise large amounts of elemental iron (3.8–6.1% by XPS and 36–43% by EDX), much higher than that (1.0% by XPS and 11% by EDX) in the ceramic **2**, which was prepared by

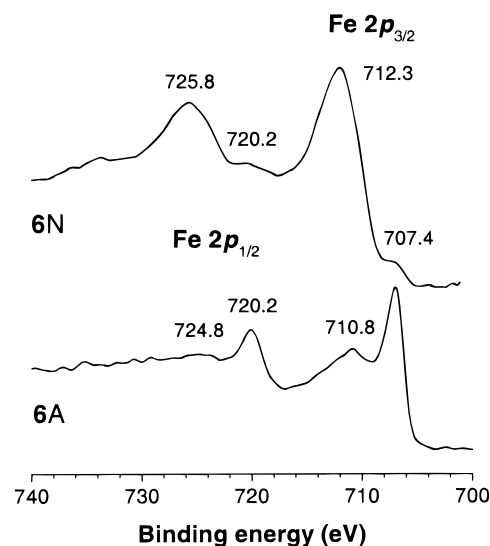


**Figure 3.** Fe 2p photoelectron spectra of ceramics **6N** and **6A**.

**Table 2. Binding Energies of Fe 2p Core Levels in Ceramics 6 and Other Fe-Containing Materials**

material	binding energy (eV)				ref		
	Fe 2p <sub>3/2</sub>		Fe 2p <sub>1/2</sub>				
<b>6</b>	707.4	710.8	712.3	720.2	724.8	725.8	this work
Fe	707.3			720.3			13
Fe <sub>3</sub> Si	707.5						13–15
Fe <sub>3</sub> O <sub>4</sub>		710.8			724.7		12
Fe <sub>2</sub> O <sub>3</sub>			711.6			725.1	12

the pyrolysis of the linear polymer **1** at a similarly high temperature (1000 °C).<sup>4</sup> The ferrocenylene moieties of **5** are confined in the roughly spherical cage of the hyperbranched polysilyne, allowing the iron species to have more time to take part in the cross-linking reaction, hence enhancing their chances to transform into nonvolatile inorganic structures.

The valence shell electrons are known to contribute to the net force experienced by the core level electrons, and the core-level binding energies thus change with the change in the chemical environments.<sup>12</sup> We inspected the Fe 2p core level photoelectron spectra of **6** (Figure 3) in an effort to understand the chemical structure of the iron species in the ceramic products. The spectrum of **6N** shows a small peak at 707.4 eV, which may be assigned to the Fe 2p<sub>3/2</sub> core-level binding energy of Fe and Fe<sub>3</sub>Si, because the literature data for the two iron species are almost identical, being respectively 707.3 and 707.5 eV (Table 2).<sup>13,14</sup> Allen et al.<sup>13</sup> and Fradley<sup>14</sup> reported a binding energy of 720.3 eV for the Fe 2p<sub>1/2</sub> line, and the peak at 720.2 eV in Figure 2 thus further confirms the existence of the elemental iron in its metallic form in **6N**.

Many research groups have investigated the Fe 2p spectra of Fe<sub>2</sub>O<sub>3</sub>. Mills and Sullivan,<sup>12</sup> for example, reported binding energies of 711.6 and 725.1 eV for the Fe 2p<sub>3/2</sub> and Fe 2p<sub>1/2</sub> peaks, respectively, and the value

(12) Mills, P.; Sullivan, J. L. *J. Phys. D: Appl. Phys.* **1983**, *16*, 723.

(13) Allen, G.; Curtis, M.; Hopper, A. J.; Tucker, P. M. *J. Chem. Soc., Dalton Trans.* **1974**, *14*, 1525.

(14) Fradley, C. S. In *Electron Spectroscopy*; Shirley, D. A., Ed.; North-Holland: Amsterdam, 1972; pp 781–801.

(15) *Handbook of X-ray Photoelectron Spectroscopy*; Chastain, J., Ed.; Perkin-Elmer: Eden Prairie, MN, 1992.

(11) Porte, L.; Sartre, A. *J. Mater. Sci.* **1989**, *24*, 271.

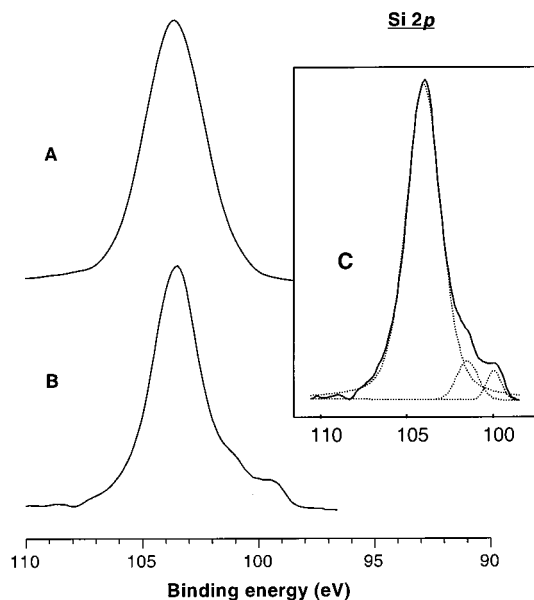


**Figure 4.** Si 2p photoelectron spectra of ceramics (A) **6N** and (B) **6A**; inset (C): curve fitting of spectrum B.

**Table 3. Binding Energies of Si 2p Core Levels in Ceramics 6 and Other Si-Containing Materials**

material	binding energy (eV)			ref
<b>6</b>	104.0	101.5	99.9	this work
SiO <sub>2</sub>	104.2			18
SiC		101.1		19
Fe <sub>3</sub> Si			99.7	20

reported by Carver et al.<sup>16</sup> for the Fe 2p<sub>3/2</sub> peak was 711.5 eV. The intense peaks at 712.3 and 725.8 eV in Figure 3 are thus likely to result from the Fe<sub>2</sub>O<sub>3</sub> nanoclusters in **6N**. The Fe 2p photoelectron peaks are rather broad, probably due to the unresolved multiple splitting of the core electron peaks caused by the exchange interaction of the unpaired valence electrons.<sup>12,13,17</sup> It is known that  $\alpha$ - and  $\gamma$ -Fe<sub>2</sub>O<sub>3</sub> species possess the same binding energy,<sup>7,15</sup> and it is thus difficult, if not impossible, to distinguish whether the iron oxide in **6N** is in the  $\alpha$ - or  $\gamma$ -form on the basis of the XPS data alone.

The Fe 2p spectrum of **6A** is, however, remarkably different from that of **6N**. The Fe and Fe<sub>3</sub>Si species give sharp intense peaks at 707.4 (Fe 2p<sub>3/2</sub>) and 720.2 eV (Fe 2p<sub>1/2</sub>). Compared with the Fe<sub>2</sub>O<sub>3</sub> peaks in **6N**, the iron oxide peaks in **6A** are located in the lower binding energy region, suggesting that the average oxidation state of the iron species in **6A** is lower than +3. The oxide can be assigned as Fe<sub>3</sub>O<sub>4</sub> because the observed binding energies for the Fe 2p<sub>3/2</sub> (710.8 eV) and Fe 2p<sub>1/2</sub> peaks (724.8 eV) are almost identical to those (710.8 and 724.7 eV, respectively) of Fe<sub>3</sub>O<sub>4</sub> reported by Mills and Sullivan.<sup>12</sup> The Fe 2p<sub>3/2</sub> envelope tails into the high binding energy region, suggesting that a small amount of Fe<sub>2</sub>O<sub>3</sub> also exists in **6A**.

The Si 2p core level spectrum of **6N** gives an intense peak at 104.0 eV (Figure 4A); thus, the silicon in **6N** is oxidized and exists in the form of SiO<sub>2</sub> (Table 3). There is no obvious signal associated with iron silicide (Fe<sub>3</sub>-

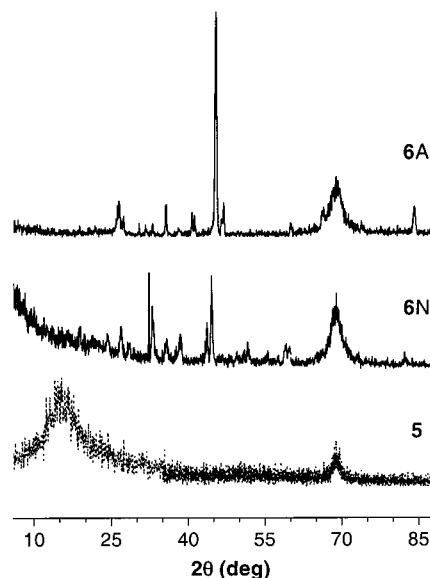


**Figure 5.** XRD patterns of poly[1,1'-ferrocenylene(methyl)silyl] **5** and its ceramic products **6N** and **6A**.

Si) possibly because the weak signal is buried under the overwhelming SiO<sub>2</sub> peak. The signal related to the Fe<sub>3</sub>-Si species is, however, detected in **6A**. The Si 2p spectrum of **6A** exhibits structured tails in the low binding energy region in addition to the main peak for SiO<sub>2</sub> (Si<sup>4+</sup>) at 104.0 eV. Using the least-squares peak-fitting program, it is resolved that the tails are the Si 2p peaks for the reduced silicon species of SiC (101.5 eV) and Fe<sub>3</sub>Si (99.9 eV)<sup>18–20</sup> (Figure 4C and Table 3).

**Crystallinity.** We used XRD diffractometry to examine the bulk composition and crystal structure of the ceramic products.

The precursor polymer **5** is amorphous, exhibiting no sharp reflection peaks but a diffuse halo in the  $2\theta$  angle region of  $\sim 5^\circ$ – $30^\circ$  (Figure 5; noticing that the broad peak centered at the  $2\theta$  angle of  $\sim 69^\circ$  is not from **5** but from the silicon wafer used in the XRD measurement). In contrast, its ceramic products **6** show diffraction patterns with numerous Bragg reflections; that is, **6** contains many crystalline species. The crystals are, however, small in size, as evidenced by the line broadening of the XRD diagrams.<sup>21</sup> Using the Scherrer equation,<sup>22</sup> it is estimated that the sizes of the crystals are in the range of 41–117 nm. The sizes of the nanocrystals are smaller than those estimated from the SEM image, suggesting that the nanocrystals coexist with other species in the nanoclusters. In other words, the nanoclusters are not pure in composition but are mixtures of different species, in agreement with the XPS

(18) Zhou, J. N.; Butera, A.; Jiang, H.; Yang, D. H.; Barnard, J. A. *J. Appl. Phys.* **1999**, *85*, 6151.

(19) Senemaud, C.; Gheorghiu-de La Rocque, A.; Dufour, G.; Herlin, N. *J. Appl. Phys.* **1998**, *84*, 4945.

(20) Shabanova, I. N.; Trapeznikov, V. A. *J. Electron. Spectrosc. Relat. Phenom.* **1975**, *6*, 297.

(21) (a) Tang, B. Z.; Geng, Y.; Lam, J. W. Y.; Li, B.; Jing, X.; Wang, X.; Wang, F.; Pakhomov, A. B.; Zhang, X. X. *Chem. Mater.* **1999**, *11*, 1581. (b) Tang, B. Z. *CHEMTECH* **1999**, *29* (11), 7. (c) Tang, B. Z.; Sun, Q.; Geng, Y.; Zhang, X. X.; Jing, X. *Pure Appl. Chem.* **2000**, *72*, 157.

(22) (a) Klug, H. P.; Alexander, L. E. *Powder X-ray Diffraction Techniques*; Wiley: New York, 1974. (b) Guinier, A. *X-ray Diffraction in Crystals, Imperfect Crystals, and Amorphous Bodies*; Dover: New York, 1994.

(16) Carver, J. C.; Schweitzer, G. K.; Carlson, T. A. *J. Chem. Phys.* **1972**, *57*, 973.

(17) Bruncl, C. R.; Chuang, T. J.; Wandelt, K. *Surf. Sci.* **1977**, *68*, 459.

**Table 4. Nanocrystals in Ceramics 6 Identified by XRD Analysis**

no.	crystal	$2\theta$ (deg)/ $d$ spacing (Å) <sup>a</sup>		ICDD file
		6N <sup>b</sup>	6A <sup>c</sup>	
1	Fe	43.65/2.07 (2.08)		31-0619
2	Fe <sub>3</sub> Si	44.55/2.03 (2.00)	45.40/2.00 (2.00), 66.35/1.41 (1.41), 84.15/1.15 (1.15)	45-1207
3	Fe <sub>3</sub> O <sub>4</sub>		35.48/2.53 (2.53)	75-1372
4	α-Fe <sub>2</sub> O <sub>3</sub>	33.00/2.71 (2.70), 35.65/2.52 (2.52), 49.50/1.84 (1.84), 54.75/1.68 (1.69)	33.00/2.71 (2.70)	33-0664
5	γ-Fe <sub>2</sub> O <sub>3</sub>	35.65/2.52 (2.51), 57.50/1.60 (1.60)		25-1402
6	SiO <sub>2</sub>	28.45/3.13 (3.11) <sup>d</sup>	30.40/2.94 (2.94) <sup>e</sup>	<i>d, e</i>
7	SiC	35.65/2.52 (2.51), 59.85/1.54 (1.54) <sup>f</sup>	35.48/2.53 (2.53), 38.05/2.36 (2.37), 59.95/1.54 (1.55) <sup>g</sup>	<i>f, g</i>
8	C	26.90/3.31 (3.35) <sup>h</sup>	26.50/3.36 (3.35) <sup>h</sup>	<i>h</i>

<sup>a</sup> The values given in the parentheses are taken from the powder diffraction files of the database of the International Center for Diffraction Data (ICDD). <sup>b</sup> Sintered under nitrogen at 1000 °C for 1 h. <sup>c</sup> Sintered under argon at 1200 °C for 1 h. <sup>d</sup> Coesite; ICDD data file 72-1601. <sup>e</sup> Stishovite; ICDD data file 72-2310. <sup>f</sup> Carborundum; ICDD data file 73-1708. <sup>g</sup> ICDD data file 75-1541. <sup>h</sup> Graphite; ICDD data file 75-2078.

and EDX results discussed above. The nanocrystals are, however, larger than the iron nanoclusters in the ceramics prepared by Manners and Ozin's groups (~2–20 nm).<sup>4,5</sup> One possible reason for the difference is the higher metal content of **5**, which enables the inorganic nanocrystals in **6** to grow bigger during the ceramization process. It is well-known that large surface effect adversely contributes to the reduction in the magnetizability of small magnetic nanoclusters<sup>21</sup> and it is expected that the ceramics **6** with large magnetic nanocrystals will show high magnetizability. This is indeed the case, as will be discussed in detail in the next section.

We used the data files in the database of the Joint Committee on Powder Diffraction Standards of the International Center for Diffraction Data (JCPDS-ICDD) to identify the nanocrystals, and the results are summarized in Table 4. The ceramic **6N** shows reflection peaks of Fe and Fe<sub>3</sub>Si crystals at  $2\theta = 43.65^\circ$  ( $d = 2.08$  Å) and  $44.55^\circ$  (2.03 Å), respectively. Their secondary reflections can, however, not be detected, probably due to the imperfect packing structure of the nanocrystals.<sup>22</sup> The diffraction diagram of **6N** displays a peak of α-Fe<sub>2</sub>O<sub>3</sub> at  $2\theta = 33.00^\circ$  (2.71 Å), whose higher order reflections are observed at  $35.65^\circ$  (2.52 Å),  $49.50^\circ$  (1.84 Å), and  $54.75^\circ$  (1.68 Å), implying that the α-Fe<sub>2</sub>O<sub>3</sub> nanocrystal in **6N** still holds a regular packing structure (Table 4, no. 4). The reflection peaks associated with the γ form of Fe<sub>2</sub>O<sub>3</sub> at  $35.65^\circ$  (2.52 Å) and  $57.50^\circ$  (1.60 Å) are, however, weak in intensity. Thus, while the XPS analysis provided no clear information on the crystal polymorph, the XRD analysis here reveals that the Fe<sub>2</sub>O<sub>3</sub> nanocrystals exist mainly in the α form. The reflection peaks of SiO<sub>2</sub>, SiC, and C are all weak and broad, probably because the majority of the silicon and carbon species is in the irregular amorphous state.

In the XRD diagram of **6A**, we cannot find any peaks associated with the reflections of Fe metal. An intense peak of the Fe<sub>3</sub>Si nanocrystal is, however, observed at  $45.40^\circ$  (2.00 Å), whose higher order reflections are clearly identifiable at  $66.35^\circ$  (1.41 Å) and  $84.15^\circ$  (1.15

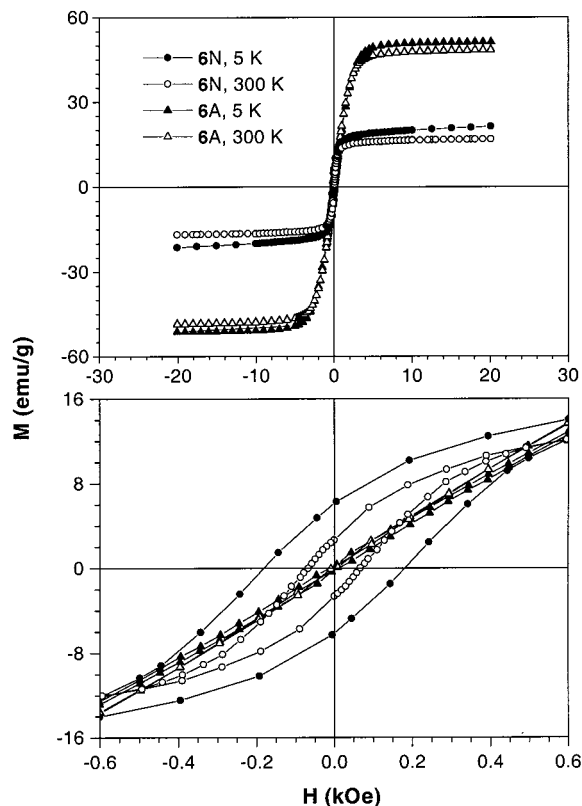


**Figure 6.** Plots of magnetization ( $M$ ) versus applied magnetic field ( $H$ ) at 5 and 300 K for ceramics **6N** and **6A**, the lower panel being the enlarged part of the magnetization curves in the low magnetic field region.

Å). Thus, most, if not all, of the iron species in **6A** exist in the form of Fe<sub>3</sub>Si. Consistent with the XPS data, **6A** shows an Fe<sub>3</sub>O<sub>4</sub> peak of moderate intensity at  $35.48^\circ$  (2.53 Å) but only a weak peak of α-Fe<sub>2</sub>O<sub>3</sub> at  $33.00^\circ$  (2.71 Å). This is in contrast to the XRD diffraction pattern of **6N**, in which no Fe<sub>3</sub>O<sub>4</sub> but α-Fe<sub>2</sub>O<sub>3</sub> peaks are observed (Table 4, nos. 3–4). The reflections of the SiO<sub>2</sub>, SiC, and C species in **6A** are again weak and broad, probably due to the same reasons as discussed above for **6N**.

**Magnetism.** The ceramic products **6** can be readily attracted to a bar magnet at room temperature; that is, they are readily magnetizable. We thus used the SQUID technique to investigate their magnetization behaviors in magnetic fields.

As shown in the upper panel of Figure 6, at 300 K, **6N** is magnetized even when a weak magnetic field is applied. Its magnetization increases with an increase in the strength of the applied field and becomes saturated at ~16 emu/g when the external field reaches ~2 kOe. Its  $M_s$  increases to ~21 emu/g when the temperature is decreased to 5 K. The  $M_s$  for **6A** at this temperature is, however, ~51 emu/g, which is ~2.5-fold higher than that for **6N**. The XPS and XRD analyses have revealed that Fe<sub>3</sub>Si is the major component of the nanocrystals in **6A**, while in **6N**, the nanocrystals are mainly α-Fe<sub>2</sub>O<sub>3</sub>, with γ-Fe<sub>2</sub>O<sub>3</sub>, Fe, and Fe<sub>3</sub>Si existing in relatively small quantities. Fe<sub>3</sub>Si, γ-Fe<sub>2</sub>O<sub>3</sub>, and Fe are the best-known magnetic materials but α-Fe<sub>2</sub>O<sub>3</sub> is only weakly magnetic;<sup>23</sup> **6A** thus should show higher

(23) Pham-Huu, C.; Estournes, C.; Heinrich, B.; Ledoux, M. J. *J. Chem. Soc., Faraday Trans.* **1998**, *94*, 435.

magnetizability than **6N**. The SQUID measurements prove that this is indeed the case, reinforcing the composition analyses of the ceramics by the XPS, EDX, and XRD techniques.

When the portion of the magnetization plots in the low-field region is enlarged, the hysteresis loops of **6N** become clearly visible. Its  $M_r$  and  $H_c$  values at 300 K are, however, very low, being only 2.6 emu/g and 65 Oe, respectively. When the temperature is decreased to 5 K, the  $M_r$  and  $H_c$  values increase to 6.4 emu/g and 180 Oe, respectively. The remanence and coercivity of **6N** are possibly due to the contribution from its  $\gamma$ -Fe<sub>2</sub>O<sub>3</sub> component.<sup>21</sup> Typical  $H_c$  values for bulk  $\gamma$ -Fe<sub>2</sub>O<sub>3</sub> maghemite are 250–400 Oe.<sup>24</sup> The  $H_c$  values for **6N** are much lower (65–180 Oe), probably due to the imperfect structure, the surface effect,<sup>21</sup> and/or the small amount of the  $\gamma$ -Fe<sub>2</sub>O<sub>3</sub> nanocrystals in the ceramic product.

Interestingly, however, even at high magnification, **6A** does not seem to exhibit any hysteresis loops and its magnetization curves nearly cross the zero point (i.e.,  $M_r \sim 0$ ,  $H_c \sim 0$ ), when the magnetization experiments are carried out at both 300 and 5 K. Silicon steel (Si–Fe) is widely used in electromagnetic systems because of its extremely low magnetic hysteresis loss.<sup>25</sup> The near-zero  $M_r$  and  $H_c$  values of **6A** are easy to understand because Fe<sub>3</sub>Si is the major component of the nanocrystals in the ceramic product. Thus, **6A** is an excellent soft ferromagnetic material with high magnetic susceptibility and low hysteresis loss.

### Concluding Remarks

In summary, in this study, we have successfully prepared mesoporous magnetoceramic materials using hyperbranched organometallic polymer precursors. We have observed that (1) the ceramization yield increases with a decrease in the alkyl chain length of the hyperbranched poly[1,1'-ferrocenylene(*n*-alkyl)silylene] precursors, with the highest yield obtained in the polymer with the smallest alkyl (methyl) group; (2) the hyperbranched polysilylenes are superior to their linear polysilylene counterparts in terms of the pyrolytic conversion to inorganic networks and the retention of elemental iron in the ceramic products; (3) the simultaneous evaporation of volatile organics and agglomeration of inorganic elements in the pyrolysis of **5** readily generates a three-dimensional mesoporous network of nanoclusters; and (4) the iron silicide nanocrystals make **6A** an excellent soft ferromagnetic material, exhibiting a high magnetizability and a negligibly small hysteresis loss.

The information gained in this work is useful in terms of guiding molecular engineering endeavors in the design of molecular structures of precursor polymers. Our study suggests such an "ideal" molecular structure for an organometallic polysilylene precursor: "high branching density + small substituents on silicon". Thus,

(24) (a) Zhang, L.; Papaefthymiou, G. C.; Ying, J. Y. *J. Appl. Phys.* **1997**, *81*, 6892. (b) Kang, Y. S.; Risbud, S.; Rabolt, J. F.; Stroev, P. *Chem. Mater.* **1996**, *8*, 2209. (c) Mørup, S.; Mødker, F.; Hendriksen, P. V.; Linderoth, S. *Phys. Rev. B* **1995**, *52*, 287.

(25) (a) *Power Electronics in Transportation*; Power Electronics Society: Piscataway, NJ, 1998. (b) Nie, H. *Giant Magnetoimpedance Effects in Soft Ferromagnetic Materials*; M. Phil. Thesis, Hong Kong University of Science & Technology, 1998. (c) *Proceedings of the 10th International Conference on Soft Magnetic Materials*; Muller, M., Ed.; North-Holland: Amsterdam, 1992. (d) Chen, C.-W. *Magnetism and Metallurgy of Soft Magnetic Materials*; Dover: New York, 1986.

replacing the methyl group in **5** with a hydrogen atom, which is small yet reactive,<sup>1,9</sup> should lead to the high-yield production of a ceramic material with high iron content.

The pyrolysis process provides a fast and simple route for the preparation of mesoporous ceramic materials. While the spatial distribution of the nanoclusters in **6** is random, we are extending our efforts to the design and synthesis of amphiphilic copoly(ferrocenylene-silylenes), in the hope of converting the self-assembled nanostructures of the copolymers to well-ordered mesoporous morphologies by controlled pyrolysis.<sup>2a,5,26,27</sup>

The mesoporous structure, coupled with other properties inherent with ceramic materials (thermal stability, mechanical strength, solvent resistance, etc.), makes **6** promising candidates for many practical applications. For example, **6** may be used as high-temperature filters or separation membranes, whose three dimensionally tortuously interconnected pathways offers the advantage of decreasing the likelihood of the mesopores being clogged by filtrates.<sup>28</sup> The high surface areas associated with the mesoporous structures may be utilized in the supported catalysis; that is, **6** may be used as matrix nanomaterials for embedding catalytic species in the preparation of efficient and reusable catalysts.

The soft ferromagnetism of **6** may also find technological applications in many areas<sup>29</sup> such as information storage and magnetic refrigeration. The nanostructured magnetoceramic materials are electrically highly conductive, further investigation of which may lead to the development of novel electromagnet devices of nanodimensions, for example, nanomotors<sup>30</sup> and nanoswitches.

**Acknowledgment.** The work described in this paper was partially supported by the grants of the Research Grants Council of the Hong Kong Special Administrative Region, China (Project HKUST6187/99P, 6062/98P, and 6149/97P). This project has also benefited from the support of the Joint Laboratory for Nanostructured Materials and Technology between the Chinese Academy of Sciences and the Hong Kong University of Science & Technology (HKUST). We thank Dr. Keith Moulding of the Materials Characterization and Preparation Facility (MCPF) of HKUST for technical assistance. We also thank Mr. Jiaqi Zheng of MCPF and Dr. Jianxiong Li of the Department of Chemical Engineering of HKUST for their helpful discussions.

CM000094B

(26) (a) MacLachlan, M. J.; Manners, I.; Ozin, G. A. *Adv. Mater.* **2000**, *12*, 675. (b) Power-Billard, K. N.; Manners, I. *Macromolecules* **1990**, *23*, 26. (c) Massey, J. A.; Power, M. A.; Winnik, M. A.; Manners, I. *Adv. Mater.* **1998**, *10*, 1559.

(27) Dagoni, R. *Chem. Eng. News* **1999**, *77*, 25.

(28) Kinning, D. J.; Thomas, E. L.; Ottino, J. M. *Macromolecules* **1987**, *20*, 1129.

(29) (a) Audram, R. G.; Huguenard, A. P. U.S. Patent 4 302 523, 1981. (b) Rosensweig, R. E. *Ferrohydrodynamics*; MIT Press: Cambridge, 1985. (c) Ziolo, R. F.; Giannelis, E. P.; Weinstein, B. A.; O'Horo, M. P.; Ganguly, B. N.; Mehrotra, V.; Russell, M. W.; Huffman, D. R. *Science* **1992**, *257*, 219. (d) McMichael, R. D.; Shull, R. D.; Swartzendruber, L. J.; Bennett, L. H.; Watson, R. E. *J. Magn. Magn. Mater.* **1992**, *111*, 29. (e) Marchessault, R. H.; Richard, S.; Rioux, P. *Carbohydr. Res.* **1992**, *224*, 133. (f) Pope, N. M.; Alsop, R. C.; Chang, Y.-A.; Sonith, A. K. *J. Biomed. Mater. Res.* **1994**, *28*, 449. (g) Bhatnagar, S. P.; Rosensweig, R. E. *J. Magn. Magn. Mater.* **1995**, *149*, 198.

(30) (a) Tang, B. Z.; Xu, H. *Macromolecules* **1999**, *32*, 2569. (b) Tang, B. Z.; Xu, H. In *Physics and Chemistry of Nanostructured Materials*; Yang, S., Sheng, P., Eds.; Taylor & Francis: London, 2000; pp 121–139.